Chapter 2

Materials and Methods

CHAPTER 2: Materials and Methods

2.1 Overview

Objective details are discussed in Chapter 1, it is important to describe the process and characterization of the synthesis of materials using various tools, and to apply experimental techniques for their properties and applications. The proposed materials in the present investigation are (a) $CsPbBr_xI_{(3-x)}$ (x = 0.0 to 3.0, in the step size of 0.5) (b) Cesium tin bromide ($CsSnBr_3$) (c) Cs_2PbBr_4 and Cs_2SnBr_4. All materials were prepared by the cold sintering method via solid-state reaction (SSR) route and thin films of these samples were deposited by Pulsed Laser Deposition (PLD) technique. Moreover, a spin coater has also been used for making thin films. The structural, thermodynamical, electrical, and optical properties are investigated for synthesized materials. This chapter is divided into three parts:

(a) Synthesis of compounds: The material synthesis and processing of compositions have been explained in this part.

(b) Characterizations: The structural, electrical, thermodynamical, and optical characterization techniques have been explained in this part.

(c) Data analysis: Such as Rietveld refinement to identify the phase formation of materials, electrical conductivity, and impedance spectroscopy have been discussed in this section.

2.2 Synthesis of Compounds:

2.2.1 Specification of the Materials

The raw materials with high purity were used to synthesize the various perovskite compounds. Table 2.1 represents the detail of the materials with their purity, chemical formula, and manufacturer.

Table 2.1: Details of the raw materials

S. No	Raw Materials	Chemical Formula	Purity	Manufacturer
1.	Cesium bromide	CsBr	99.999% and 99.9%	Sigma Aldrich and Alfa Aesar
2.	Lead bromide	$PbBr_2$	98%	Sigma Aldrich
3.	Cesium Iodide	CsI	99.9%	Sigma Aldrich
4.	Lead Iodide	PbI_2	98%	Synthesize in Lab
5.	Tin(II) bromide	$SnBr_2$	99.2%	Alfa Aesar

Moreover, some reagents, chemicals, and solvents such as hydrochloric acid, dimethylformamide (DMF), nitric acid, lead nitrate, potassium iodide, ethanol, isopropanol, acetic acid, etc were also used to fabricate the compounds. There are various methods to synthesize the perovskite materials (active materials) such as vapor-assisted solution process, one-step deposition, two-step deposition, solvent engineering, etc [117],[118],[119]. Most of the work was done in an inert atmosphere. Furthermore, the synthesis of halide perovskite is

not easy despite several synthesis techniques. As discussed in Chapter 1, halide perovskites are not stable and are difficult to synthesize under ambient conditions. Therefore, there is a need to understand the issue of stability and why synthesis of these materials is difficult under ambient conditions. It is observed that the cold sintering method is the easiest and low-cost synthesis as compared to other reported synthesis methods, in which the material can be synthesized under ambient conditions. All the synthesis methods are discussed in the next section which was used in the present investigation.

2.2.2 Cold Sintering Method via Solid State Reaction Method (SSR)

Cold sintering is the synthesis process that recommends low-temperature synthesis (up to 200 ^{o}C). In the conventional sintering process, synthesis occurs via phase formation, recrystallization, and grain growth. While in cold–sintering, phase formation, recrystallization, and grain growth occur up to 200 ^{o}C without any calcination [120]. Here, in the case of perovskite halides, the nucleation temperature is lower than the room temperature., hence, can be used for the synthesis. This is the easiest and low-cost synthesis method than other reported synthesis methods and provides good stability at room temperature.

2.2.2.1 Synthesis of Materials

Cesium lead halides and cesium lead-free halides have been synthesized by the cold sintering method in ambient conditions (Fig. 2.1). For synthesizing the $CsPbBr_xI_{3-x}$ (x = 0.0 to 3.0, in the step size of 0.5) $CsSnBr_3$, Cs_2PbBr_4 and Cs_2SnBr_4, the precursors of CsBr, CsI, PbI_2, $PbBr_2$, $SnBr_2$ has been weighed in stoichiometric quantities. To prepare the special compound, the desired precursors in powder form were mixed (Humidity, 34 %) in a pestle mortar and crushed for two hours at room temperature. After grinding, a hydraulic press was used for the

pelletization of perovskite powder (active material). Finally, heat the pelleted samples in a vacuum oven at 80 °C for 1 h.

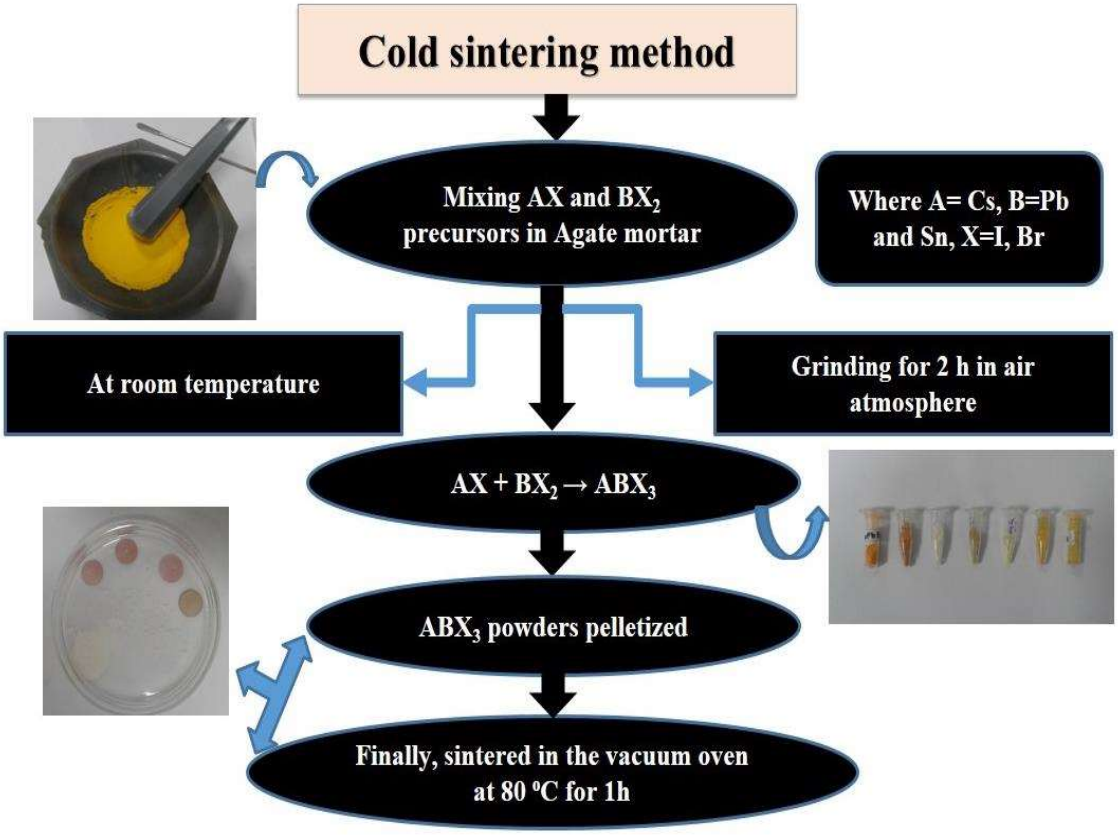

Figure 2.1: Flow chart of cold sintering method for synthesizing the perovskite samples.

In addition, $Pb(NO_3)_2$ and KI powders were weighed in stoichiometric quantities to synthesize PbI_2. The chemical reaction is given below.

$$Pb(NO_3)_2 + 2KI \rightarrow PbI_2 + 2KNO_3$$

Lead nitrate and potassium iodide were taken with distilled water in two separate beakers and the solutions of both beakers were heated to boiling point on a hot plate with a stirring rate of 550 rpm. Further, lead nitrate and potassium iodide has been mixed in another beaker. After that, the mixer of lead nitrate and potassium iodide was kept for natural cooling and found the

yellow precipitate of PbI_2 (shown in Fig. 2.2). This yellow precipitate has been filtered and heated in the vacuum oven at 100 °C for a few hours to remove the water solution.

Figure 2.2: Yellow precipitate of lead iodide.

2.2.3 Thin Films Synthesis

2.2.3.1 Spin Coating Technique

It is used to deposit a thin solid layer of the desired material from the solution on the substrate. Spin coating is used in organic electronics, nanotechnology, the technology sector, and a wide variety of industries [121]. The image of the spin coating unit which used in the present work is shown in Fig. 2.3.

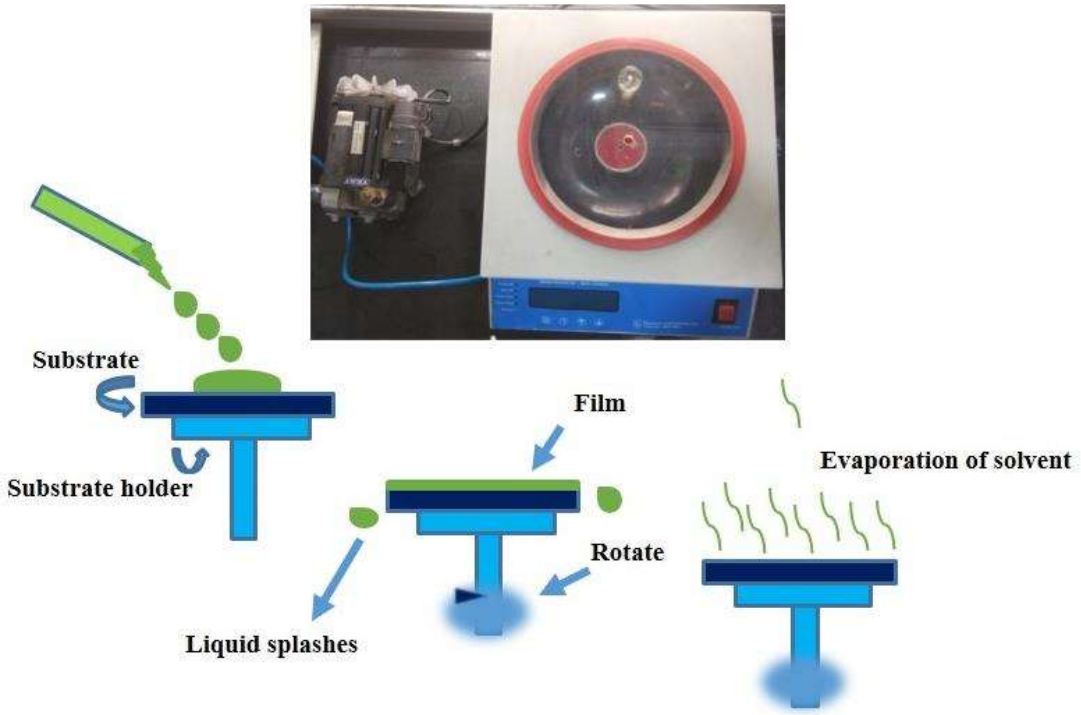

Figure 2.3: Image of the thin-film process by spin coating system.

In the spin coating process, centrifugal force is generated by the rotational motion of the substrate, causing the solution to spread outward from the center of the substrate. The surface tension of the solvent holds the solution together while the centrifugal force pulls it apart. Airflow inside the spin-coating chamber is then partially dried in the solution and also covers the thickness of a plasticized film on the resulting substrate. Various parameters affect the deposition process for uniform thin film formation such as acceleration, evaporation, the viscosity of the solution, spin speed, and spin time [122].

2.2.3.2 Pulsed Laser Deposition (PLD)

PLD is a technique to deposit the thin film on the substrate. The laser beam is used to ablate the material inside a vacuum chamber for depositing the thin film on the substrate.

Various laser sources such as XeCl (308 nm), KrF (248 nm), Nd-YAG laser, etc are being utilized to ablate the material [123].

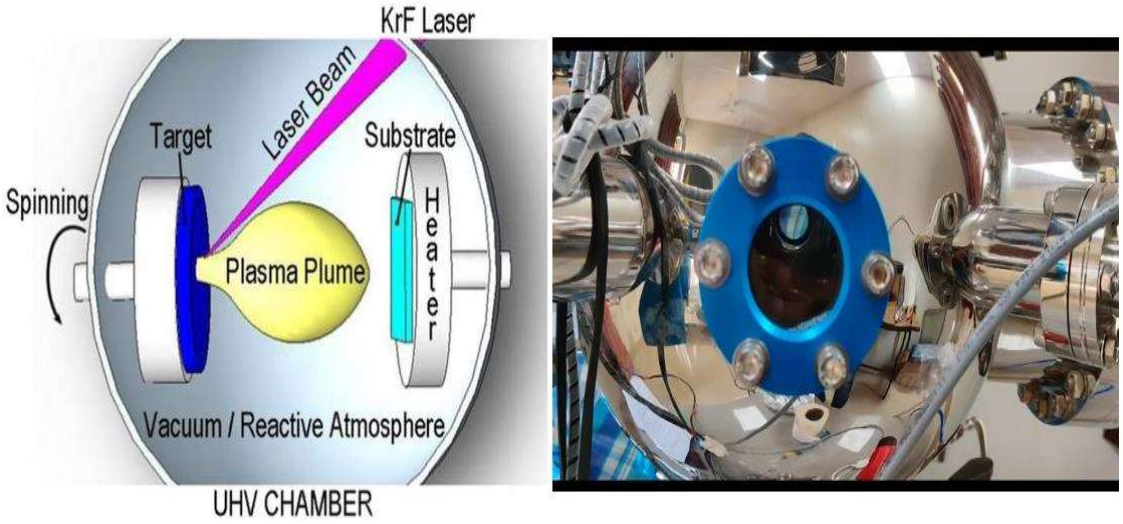

Figure 2.4: Schematic diagram of Pulsed Laser Deposition and experimental setup.

Here, cesium lead halides and cesium lead-free halides thin film were deposited by the KrF (248 nm) laser source. When a high-power pulsed laser beam strikes the target material inside the vacuum chamber then the material is vaporized from the target in the form of a plasma plume. It deposits the thin film on the various substrates. The thin film quality depends on various parameters such as ambient gas pressure, pulse duration, the wavelength of the laser, the distance of the target material to the substrate, etc. In this thesis work, the thin films were deposited by the PLD, and the image of PLD is represented in Fig 2.4.

2.3 Characterization Techniques (Measuring Equipment and Experiment Analysis Techniques)

2.3.1 X-Ray Diffraction (XRD)

The phase formation and other structural parameters of the materials such as average grain size, crystallinity, etc can be investigated by XRD. It is a non-destructive and versatile analytical technique in which the materials can also be exposed to different temperature and pressure conditions during the collection of the diffraction pattern [124]. XRD peaks are generated by constructive interference of a monochromatic beam of X-rays scattered at specific angles from each set of lattice planes in a material. Constructive interference appears when the path lengths of rays diffracted from different planes differ by multiple wavelengths. The radiation from the X-ray source strikes the material and is diffracted in all directions. The regular pattern for the atomic arrangements in a crystalline material is observed due to interference of rays diffracted from different crystalline planes. The peak intensities are identified by the atomic positions within the lattice planes.

The principle of X-ray diffraction measurements is based on the scattering of electromagnetic waves (X-rays) on structures in the range of 1 Å (shown in Fig. 2.5). The X-ray diffraction (XRD) method follows Bragg's law ($2d\sin\theta = n\lambda$) to examine various characteristics of the polycrystalline or crystal material. Where θ is the scattering angle, λ is the wavelength of X-ray, d is the distance between the structural planes, and n is the order of diffraction pattern.

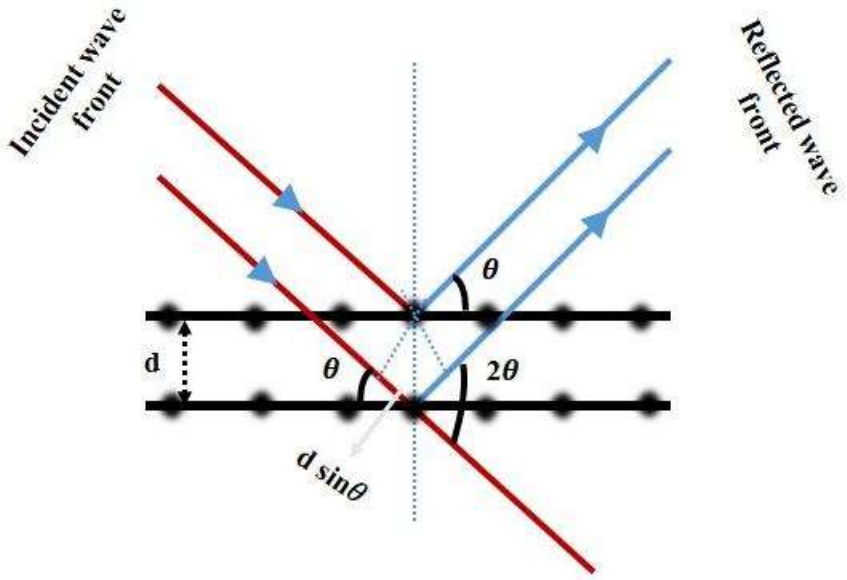

Figure 2.5: Two parallel incident X-rays reflected from crystalline planes.

The diffracted beam thus fulfills the geometry of a reflection but originates only for a specific discrete value of θ for which Bragg's law is fulfilled. Since, $(\sin\theta)_{max} = 1$. Using Bragg's law ($2d\sin\theta = n\lambda$) equation.

$$\frac{n\lambda}{2d} \leq 1 \qquad 2.1$$

This equation represents that λ should not exceed twice the interplanar spacing, otherwise, there would be no diffraction.

In some cases, the X-ray source is kept stationary while the sample and detector are rotated by θ and 2θ, respectively. However, the sample retains a stationary position in most cases while both the detector and source are simultaneously rotated by θ angle. The central part of the diffractometer is the Goniometer, and such precise rotation is performed. Generally, the sample has been mounted on a rotational axis, and the detector and X-ray source moves along

its periphery. Usually, the 2θ range between 20° - 80° is sufficient to cover the most useful part of the diffraction pattern.

The identification of the phase formation for the synthesized samples was performed by the X-ray Diffractometer (Rigaku Miniflex) with Cu-Kα radiation (λ=1.540598 Å) in the 2θ range of (5^o-70^o) at room temperature. The XRD data were recorded with a slow-scanning rate (2^o degree/minute) in a step size of 0.01 degree with an applied voltage of 40 kV and a current of 15 mA. In the present work, an X-ray diffractometer (Rigaku Miniflex, Japan) was employed to study the synthesized material (shown in Fig. 2.6).

Figure 2.6: X-ray diffractometer (Rigaku Miniflex, Japan), CIF IIT (BHU).

2.3.2 Differential Scanning Calorimetry (DSC)

It provides useful information about the thermal transition occurring in the material. Moreover, Differential scanning calorimetry detects the exothermic and endothermic processes occurring in a sample by measuring the amount of heat absorbed or released during heating or cooling of the material [125]. This technique uses two small identical sample holders; One

holds the test sample in a sealed small aluminum (Al) pan, and the other has an empty reference pan. The temperature of two samples is measured with two identical platinum-resistance thermistors. It measures the difference in heat flow rate (mW) between material and reference as a function of temperature and time. During the experimental process, both the sample and the reference are kept at approximately the same temperature. The temperature program in this analysis is designed such that the temperature of the material holder increases linearly as a function of time and the reference sample should have well-defined heat capacity over the entire range of temperatures that have to be scanned. Determination of specific heat capacity is one of the most important applications of DSC. The DSC technique can also calculate reaction enthalpies (ΔH), Gibbs free energy (ΔG), and reaction rates.

$$H = U + pV, \tag{2.2}$$

$$G = H - TS, \tag{2.3}$$

where, *U, p, V, S,* and *T* are the internal energy, pressure, volume of the system, entropy, and the temperature in kelvin, respectively.

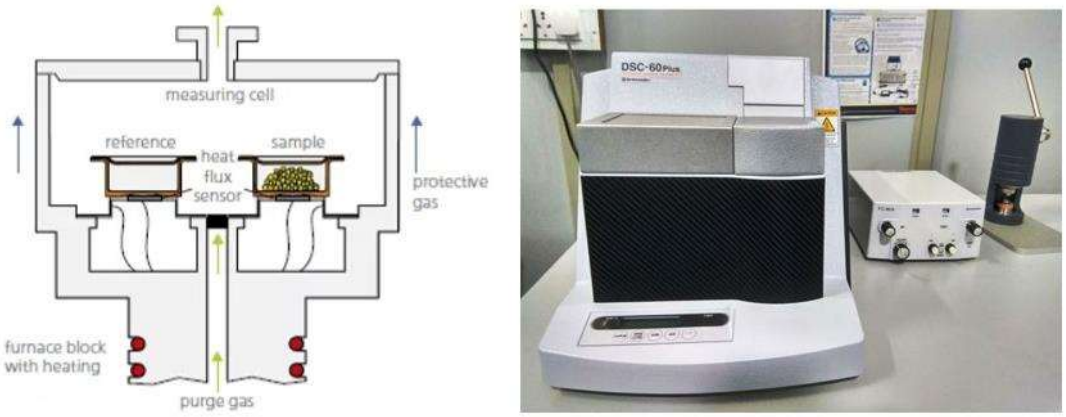

Figure 2.7: The working principle (left) and the experimental setup of DSC (right), CIF IIT (BHU).

It provides a curve of heat flux versus temperature or time. In the present thesis work, DSC measurement was taken by SHIMADZU DSC-60 plus 230V. The various parameters such as entropy, enthalpy, type of reaction, specific heat, and Gibbs free energy of the samples were analyzed. DSC is used in a broad range of industries and research areas for the investigation of the melting point of crystals, glass transition, phase transition, crystallization temperatures, chemical reactions, etc. The schematic diagram and experimental setup of the DSC technique (depicts in Fig. 2.7).

2.3.3 X-Ray Photoelectron Spectroscopy (XPS)

The surface chemical composition of the surface of a sample, electronic state, and oxidation state can be examined by XPS. In addition, which elements are present in the sample, in which oxidation state, and in which concentration can also be observed by the X-ray photoelectron spectroscopy [126].

In this technique, a sample placed in an ultra-high vacuum (UHV) is irradiated with a soft X-ray (photon of energy). Then the atoms on the surface emit photoelectrons, followed by a direct transfer of energy from the photon to the core level electron. XPS can analyze a compound to a depth of (1 to 10 nm). The XPS measurement is conducted in an ultra-high vacuum (UHV $\approx 10^{-9}$ millibar) or high vacuum (P $\approx 10^{-8}$ millibars) conditions. Some photo-ejected electrons inelastically scatter through the sample enroute to the surface in a typical XPS spectrum. In contrast, others undergo accelerated emission and escape from the surface and surrounding vacuum without any energy loss. Once these photo-ejected electrons are in the vacuum, they are collected by an electron analyzer that calculates their kinetic energy. An electron energy analyzer generates an energy spectrum of binding energy (the energy of

electrons before leaving the atom) versus intensity (number of photo-ejected electrons versus time). According to its principle, XPS can determine all the elements present in the sample. In practice, it can identify elements whose atomic number Z = 3 (lithium) and above. It cannot easily detect the atomic numbers Z=1 and 2 of elements such as hydrogen and helium.

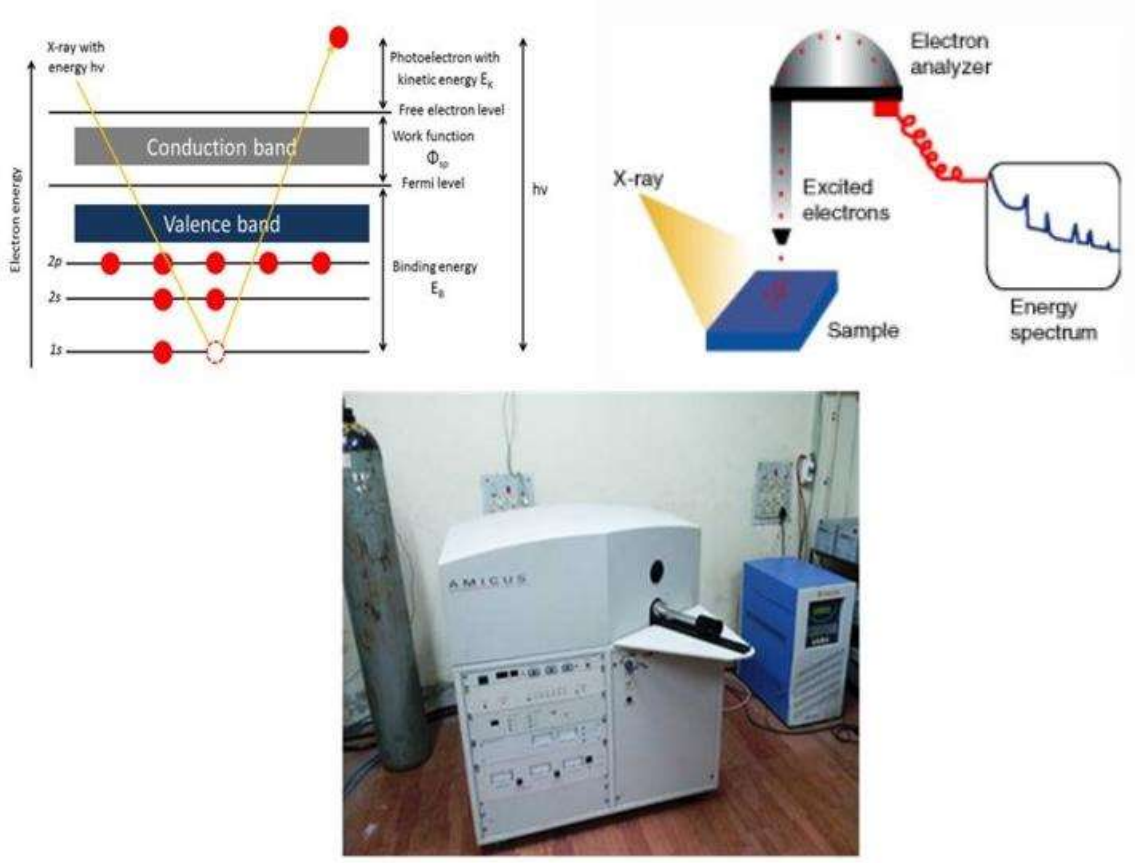

Figure 2.8: Depicts the mechanism of XPS spectroscopy and experimental setup for the XPS measurement.

This technique is used to observe the ceramics, glasses, papers, metal alloys, inorganic compounds, polymers, semiconductors, catalysts, ceramics, glasses, bio-materials, papers, woods, paints, inks, make-up, and many others. Fig. 2.8 is shown The AMICUS XPS setup and examined the chemical state and elemental analysis of the synthesized samples in the present thesis work.

2.3.4 SCANNING ELECTRON MICROSCOPE (SEM)

SEM is widely used to study morphological and surface characterization, and examine metal particles' size at the nano to microlevel scale. SEM utilizes a high-energy electron beam, but the beam is scanned over the surface, and the backscattering of the electrons is observed [127]. In addition, the Energy-dispersive X-ray analysis (EDAX or EDX) is used to analyze the elemental compositional analysis. It uses X-ray analysis to examine the elemental composition of any material up to 0.5 - 1 atomic percent sensitivity.

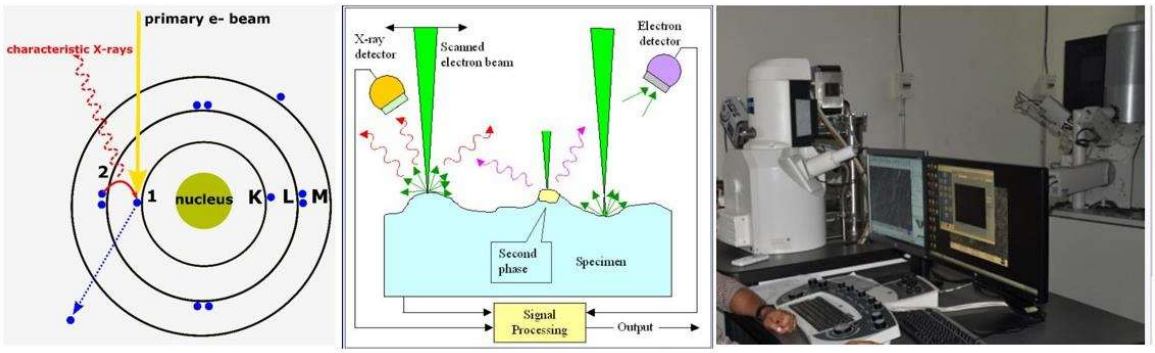

Figure 2.9: Schematic diagram of the SEM working principle and experimental setup, CIF IIT (BHU).

A high-energy electron beam is an incident on the material (sample) and an electron ejects from the inner shell of the atomic orbital of the elements present in the sample. It attracts another electron from an outer shell to fill the vacancy and this energy difference can be released in the form of X-rays. Based on the energy of this emitted X-ray, information about the elements of the sample can be obtained. X-rays are produced using EDX following a two-step process. The first is that the energy transferred to the atomic electron knocks it off, leaving behind a hole. The second is that another electron fills its position from a higher energy shell and releases a characteristic X-ray. EDAX provides semi-quantitative and qualitative

information of the elements present in any composition. In the present thesis work, SEM and EDS were recorded using EVO - Scanning Electron Microscope MA15/18, represented in Fig. 2.9.

2.3.5 Raman Spectroscopy

Raman spectroscopy is an analytical technique to identify several materials which can be liquid or gas and solid. In this technique, the vibrational energy mode of a sample is measured using scattered light. It provides both structural and chemical information, as well as identifying samples (substances) through their characteristic Raman 'fingerprints' [128]. Raman spectroscopy extracts this information by detecting Raman scattering from the sample. Raman scattering works on inelastic scattering of monochromatic light. When light interacts with the sample, the vast majority of the photons are scattered at the same energy as the incident photons, a process known as elastic scattering, or Rayleigh scattering. A small fraction of these photons, about 1 photon in 10 million, are scattered at a different frequency than the incident photon and this process is known as inelastic scattering or the Raman effect [129]. The Raman spectra of the powders have been detected in the thesis work by DXRxi Raman imaging microscope by Thermo SCIENTIFIC with the excitation wavelength of 780 nm, as shown in Fig. 2.10(a).

The working principle of the Raman spectrometer is shown in Fig. 2.10(b) which has four major components: (i) Excitation source (LASER) (ii) Sample illumination system (iii) Light collecting optics, wavelength selector (Filter, spectrophotometer) (iv) Detector (Photodiode array, CCD or Photo-multiplier-tube(PMT)). Typically, the sample is illuminated by a laser

beam of ultra-violet (UV) or visible (Vis), or near-infrared range (NIR) available with a spectrometer.

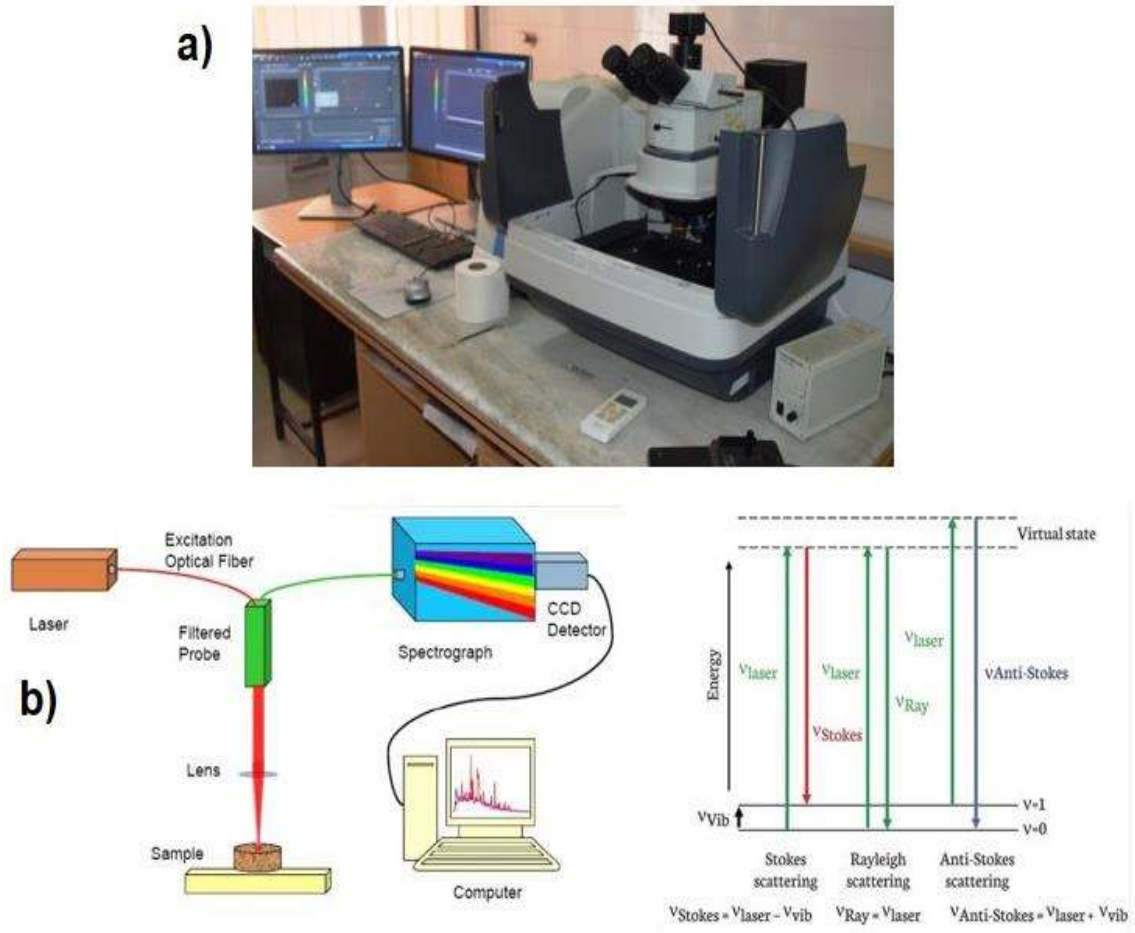

Figure 2.10: Experimental set-up of DXRxi Raman measurement. (Banasthali University, Rajasthan) (b) Schematic representation of the principle of Raman spectroscopy.

The scattered light passes through the interference filter collected by the lens to the spectrometer and records the Raman spectrum of the samples. Excitation refers to the light incident on the material by the laser source and interacting with the phonons, molecular vibrations, or other excitations present in the material. The resultant energy of the laser photon causes Raman to experience a change in the upward or downward direction. When the energy

is transferred to the higher band it is known as Anti-Stokes Raman Scattering and if the energy is shifted towards the lower band then it is known as Stokes Raman Scattering.

2.3.6 Ultra-Violet Visible (UV-Vis) Spectroscopy

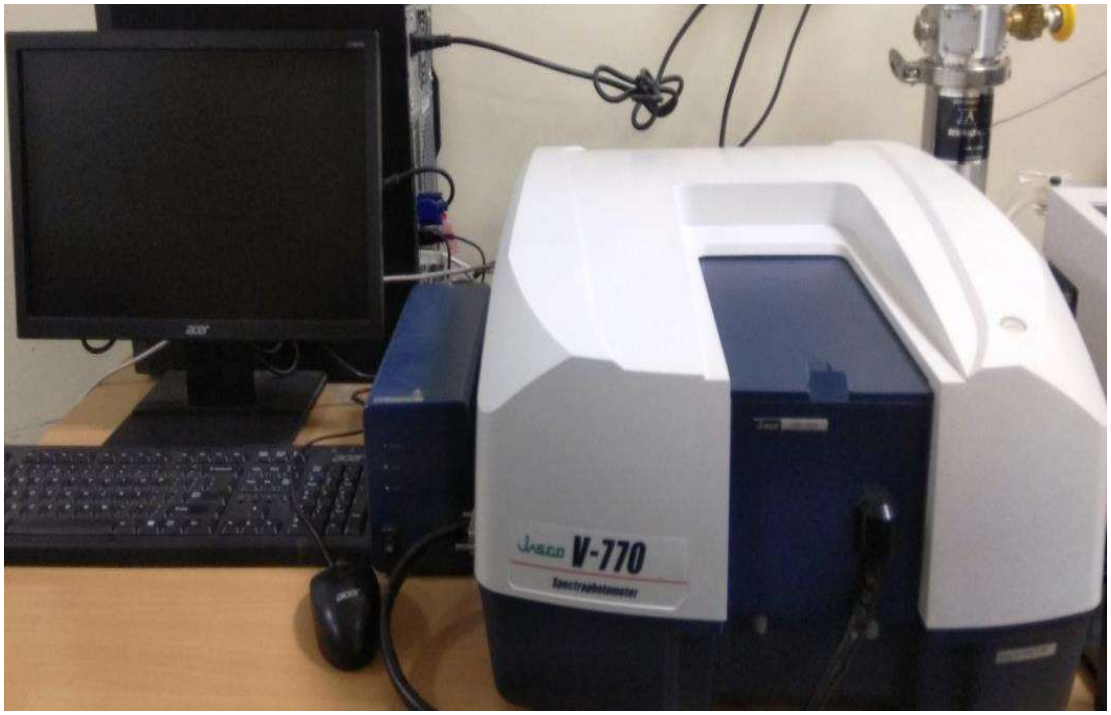

Figure 2.11: Experimental setup of JASCO V-770 UV-Vis spectrometer.

UV-Vis spectrometers have become the most important analytical tools for the investigation of optical properties of materials due to their simplicity, speed, versatility, accuracy, and cost-effectiveness. This can be observed by using UV-Vis spectroscopy to observe the absorption and reflection of samples in the ultraviolet in the visible spectral region. In addition, the bandgaps of the samples (thin films, bulk powders, liquids) have been calculated from the UV-Vis data [130].

The principle behind the operation of UV/Vis/NIR spectroscopy is Beer-Lambert's law. It is defined as the linear relation between the concentration and absorbance of absorbing material. It is given by

$$A = \log_{10}\left(\frac{I}{I_0}\right) = \varepsilon \times \ell \times c$$

Where, A, ε, b, and c are the absorbance, wavelength-dependent absorptive coefficient, path length, and material concentration, respectively. Moreover, I_0 and I are the intensity of the incident light and the intensity of the transmitted light, respectively. The spectrophotometer consists of four main components. The first is the light source, the second is the sample holder, the third is the diffraction grating of the monochromator and the fourth is the detector. The radiation source operated in continuous mode for visible wavelengths. The charge-coupled device (CCD) or photodiode, and photomultiplier tube acts as a detector. Photomultiplier tubes and single photodiode detectors are used to scan the monochromator. It filters out all wavelengths and passes only one wavelength to the detector at a time. The diffraction grating allows each wavelength to be "step-through" transferred by scanning the monochromator so that its intensity can be measured as a function of wavelength. In the present work, the absorption edge in the visible region has been observed for all the samples. JASCO V-770 ultraviolet-visible (UV) spectrometer has been used to record the optical absorption spectrum in Fig. 2.11. For the bandgap calculation of the samples, the Tauc equation has been used [131].

$$(\alpha h\nu)^{1/n} = A\left(h\nu - E_g\right)$$

where E_g, α, A, and $h\nu$ are the optical band gap, energy absorption coefficient, an energy-independent constant, and incident photon energy, respectively. 'n' is the power factor of

transition modes for direct allowed (n = 1/2), indirect allowed (n = 2), direct forbidden (n = 3/2) and indirect forbidden (n = 3) transitions.

2.3.7 Photoluminescence (PL) Spectroscopy

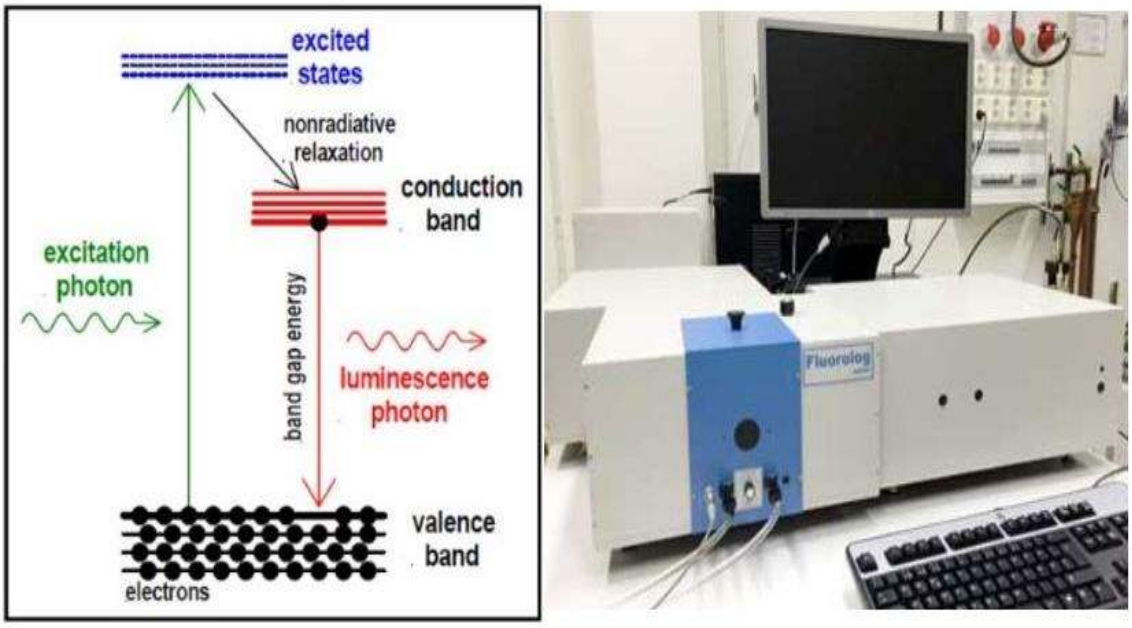

Figure 2.12: Principle of Photoluminescence spectroscopy (PL) and setup of the 450W Illuminator model FL-1039A/40A spectrometer.

PL is a useful technique to study the optical property of a sample and photoluminescence is the emission of light from any type of substance (thin film, bulk powder, liquid) after excitation from another light source. In this process, photons (electromagnetic radiation) are absorbed by matter and then re-radiate photons, and the time between absorption and emission can vary greatly from milliseconds to minutes.

Photoexcitation causes electrons within the material to move into a permissive excited state. When these electrons return to their equilibrium state, additional energy is released, and this may or may not involve the emission of light (a radiative process), as shown in Fig. 2.12.

The energy of the emitted light (photoluminescence) is related to the difference in energy levels between the two-electron states involved in the transition between the excited state and the equilibrium state. The amount of light emitted is related to the relative contribution of the radiation process. The most common radiative transition occurs between states in the conduction and valence bands in semiconductor systems, with an energy gap known as the bandgap. During the experimental process, excitation is provided by laser light with energy much higher than the optical bandgap. The photo excited carriers consist of holes and electrons, which relax towards their respective band edges and recombine by emitting light at the energy of the bandgap. Thus, PL is a process of photon excitation followed by photon emission and is used to determine the bandgap, recombination mechanism, material quality, molecular structure and crystallinity, impurity levels, and defect detection [132]. In this thesis work, the photoluminescence spectrum of the samples is measured from the 450W Illuminator model FL-1039A/40A spectrometer, as shown in Fig. 2.12.

2.4 Electrical Properties

2.4.1 Current-Voltage (*I-V*)

Keithley 2450 source meter is used to observe the current-voltage (I-V) curve of samples synthesized with AM 1.5 G filter and irradiated through Science Tech Solar Simulator of Class AAA with the high collimated beam is done, as shown in Fig. 2.13. The current response times of all samples were recorded with continuous exposure to AM 1.5 G sunlight for 3 h with darkness and room illumination. In addition, the photostability of the compounds was also observed when exposed to continuous AM 1.5 G sunlight.

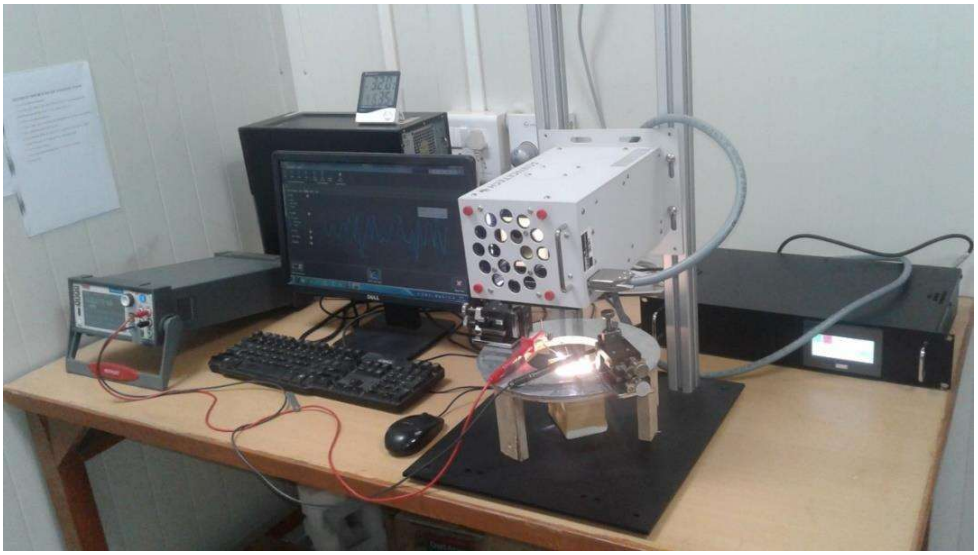

Figure 2.13: An experimental setup of a solar simulator with a Keithley source meter.

(a) Source Meter

The Keithley 2450 is a next-generation source meter or source measurement unit (SMU) instrument that measures Ohm's law (voltage, current, and resistance) with fingertip accuracy. A source meter serves as both a DC power source and a digital multi-meter. It is a multi-purpose instrument and is widely used for nanoscale devices and materials, electrical characterization of semiconductors, organic semiconductors, low-power devices, and other small geometries. This source meter act as an ohmmeter, voltage meter, current meter, current source, and voltage source. It features a five-inch high-resolution capacitive touch screen and has a native measurement accuracy of 0.012% with a 6.5-digit resolution. The front panel includes input banana jacks and the rear panel has input triaxial connections. Keithley 2450's voltage range is between 20 mV to 200V and the current range is between 10 nA-1A. Sweep can be measured in various ways like linear, log, dual linear, dual log, and custom.

(b) Solar Simulator

It provides natural light almost like sunlight. The main objective of this technology is to give a controlled indoor testing facility under laboratory conditions. Photovoltaic parameters can be separated using this technique. In addition, other tests such as plastics, other materials, and devices may be exposed to sunlight using the solar simulator. Several types of lamps such as metal halide, xenon, quartz tungsten halogen, and light-emitting diode-based lamps were used as light sources in solar simulators. But, xenon arc lamp which offers high intensity and an unfiltered spectrum that harmonizes well with sunlight. Direct radiation (comes from the sun itself) and scattered radiation (comes from the rest of the sky in which part of the radiation is reflected back to the ground) are two components of the radiation. The Solar Simulator provides the spectral distribution of sunlight for different environments and the spectral distribution from a refined and altered xenon lamp source using air mass (AM) filters. The direct radiation spectrum can be simulated using a direct filter, referred to as 'D'.

The total radiation, including scattered sky and ground radiation, can be matched using a global filter, designated as 'G' and which simulates both components simultaneously. In addition, air mass (AM) describes the length of the direct optical path through Earth's atmosphere [133]. AM 1.5 refers to the 1.5-thickness of the atmosphere which corresponds to the solar zenith angle of $z = 48.2°$. AM 1.5 is useful for describing the overall annual average for mid-latitudes. Photovoltaic devices are characterized using AM 1.5 G filters. An experimental setup of a solar simulator with a Keithley source meter is shown in Fig. 2.13.

2.4.2 Impedance Spectroscopic Technique

The electrical properties of the synthesized sample are determined by the impedance spectroscopic technique. The conductivity, dielectric, impedance, and modulus properties can

be obtained by applying an alternating voltage or current to the material. These properties include grain boundaries, grain or bulk, and electrode polarization or electrode sample contribution [134]. To optimize the useful properties and observe the electrical behavior, it is necessary to differentiate these contributions. These various contributions can be distinguished by impedance analysis present in the electrical or dielectric properties of any electronic material. Impedance analysis is an important tool to investigate the microstructure, defects, electrical conductivity, and surface chemistry of materials, including ionic conductors and dielectrics. Electrical modulus (M*), Admittance (Y*), permittivity (ε*), and complex impedance (Z*) are the four basic formalisms that allow the AC response of any compound to be expressed. These functions are related to each other as follows [135]:

$$M^* = M' + iM'' = \frac{1}{\varepsilon^*}$$

$$\varepsilon^* = \varepsilon' - i\varepsilon''$$

$$Z^* = Z' - iZ'' = \frac{1}{i\omega C_0 \varepsilon^*}$$

$$Y^* = Y' + iY'' = i\omega C_0 \varepsilon^*$$

The correlation of all these parameters to each other is given below.

$$D = \tan\delta = \frac{\varepsilon''}{\varepsilon'} = \frac{M''}{M'} = \frac{Y'}{Y''} = \frac{Z'}{Z''} = \frac{\sigma'}{\sigma''}$$

$$Z' = \frac{D^2}{G(1 + D^2)}, \qquad Z'' = \frac{Z'}{D}$$

$$\sigma' = \omega\varepsilon_0\varepsilon'' \text{ and } \sigma'' = \omega\varepsilon_0\varepsilon'$$

Where, f, ω (ω = 2π*f*), C_0 is the frequency (cycles/sec), angular frequency, and geometrical capacitance, respectively. *M′, ε′, Z′, Y′* and *M″, ε″, Z″, Y″* are the frequency-dependent real and imaginary components of the modulus, permittivity, and impedance, and admittance, respectively. In addition, Z^*, M^*, and Y^* functions are mostly used for electronic materials. If grain, grain boundary, and electrode contributions are presented in polycrystalline materials then each contribution can be represented by an R and C circuit element connected in parallel.

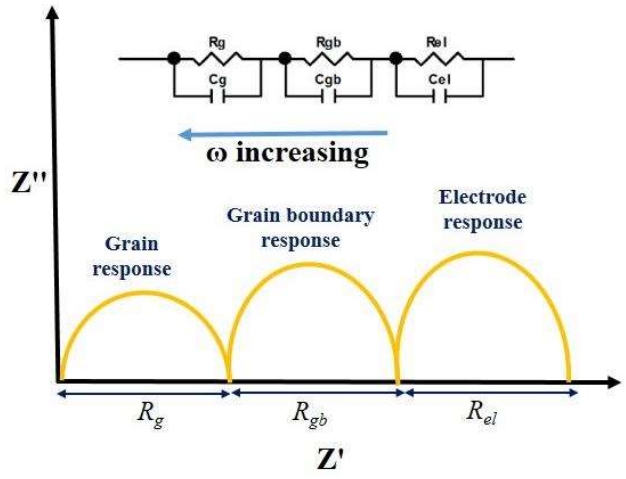

Figure 2.14: The equivalent circuit and their frequency response in the complex impedance plot.

Thus, an equivalent circuit of the sample connected three parallel RC circuits in series as shown in Fig. 2.14. The Cole-Cole or Nyquist plot is used to examine the frequency response information by the complex impedance function: $Z^*(\omega) = Z'(\omega) - iZ''(\omega)$, where $Z'(\omega)$ and $Z''(\omega)$ are the real and imaginary parts, respectively. The real (Z') and imaginary (Z") part of the total impedance of the equivalent circuit is given below.

$$Z' = \frac{R_g}{(1+\omega R_g C_g)^2} + \frac{R_{gb}}{(1+\omega R_{gb} C_{gb})^2}$$

$$Z'' = R_g \frac{\omega R_g C_{gb}}{(1+\omega R_g C_g)^2} + R_{gb} \frac{\omega R_{gb} C_{gb}}{(1+\omega R_{gb} C_{gb})^2}$$

Where, *Rg* is the grain (bulk) resistance and *Cg* is the grain capacitance, and *Cgb* and *Rgb* are corresponding quantities for the grain boundary. Grain and grain boundary contribute to low and high-frequency regions, respectively. The interfacial boundary (grain boundary) has a longer relaxation time than the bulk. R_{el} indicates the electrode polarization process while C_{el} shows their respective capacitive contribution.

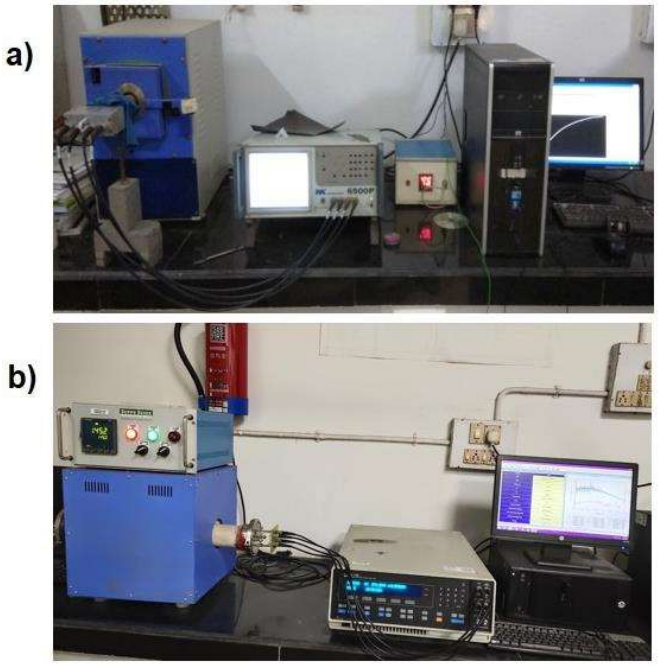

Figure 2.15: (a) Represents the experimental setup of a computer-controlled automatic impedance analyzer with sample holder and furnace. (b) Solartron 1260 A impedance analyzer.

In this thesis work, the powder samples have been pelletized by using a cylindrical disk of diameter 12 mm or 6 mm of thickness 1 to 2 mm for the electrical measurement. Silver paste has been used as electrode and finally, measurement of silver-coated pellets was obtained by two probe techniques in the air at a frequency of 20 Hz–1 MHz and invariable temperature

range using LCR meter (Wayne Kerr 6500P), as shown in Fig. 2.15(a). Moreover, the impedance measurement of the studied perovskite material was done using Solartron 1260 A impedance analyzer (Fig. 2.15 (b)).

2.5 Analysis Techniques

2.5.1 Rietveld Refinement Technique

XRD is the most effective and most frequently applied method of all the various analysis tools. R. M. Rietveld introduces a structure profile refinement technique for powder diffraction data of neutron radiation and X-rays. Rietveld refinement is an important tool for studying the structure information of samples in detail. It produces an effective separation of these overlapping data and allows an accurate assessment of the structure. Several parameters of these reflections such as width, height, and position can be used to define many aspects of the structure of the material [136]. In this process, least-squares refinement is performed to obtain the best fit of the theoretical and measured profile. Thus, a lot of information about the structure of the sample can be obtained by applying Rietveld refinement. For monochromatic neutron sources, a solution of several effects is offered to result in a Gaussian shape. If this distribution is considered, the contribution of a given reflection in the profile y_i at position $2\theta_i$ is:

$$y_i = I_k \exp\left[\frac{-4\ln(2)}{H_k^2}(2\theta_i - 2\theta_k)^2\right]$$

where, H_k, $2\theta_k$, I_k are the FWHM, a center of the reflex, the calculated intensity of the reflex (obtained from the Lorentz factor, the multiplicity of the reflection, and the structure factor), respectively. Reflection can acquire an asymmetry due to the vertical divergence of the

beam at very small diffraction angles. A_s to account for this asymmetry, Rietveld accepted a semi-empirical correction factor.

$$A_s = 1 - \left[\frac{sP\,(2\theta_i - 2\theta_k)^2}{\tan\theta_k}\right]$$

At higher Bragg angles, the width of the diffraction peaks is becoming wider. This angular dependency is formerly described by

$$H_k^2 = U\tan^2\theta_k + V\tan\theta_k + W$$

where half-width parameters (U, V, and W) can be refined during fitting by Rietveld refinement. The difference between the observed data y(obs) and a calculated profile y(calc) is evaluated by the principle of Rietveld refinement that reduces to the function M. It is given by:

$$M = \sum_i W_i \left\{ y_i^{obs} - \frac{1}{c} y_i^{calc} \right\}^2$$

where, c and W_i are an overall scale factor and the statistical weight such that $y^{calc} = cy^{obs}$, respectively. In this thesis work, the 'Fullprof Suite' program is used for performing the Rietveld refinement.

2.5.2 Process of Analyzing the Obtained Data

OriginPro 8.5 software has been used to study the sample for electrical, structural, and optical results. In addition, Image-J software was used to analyze the grain size distribution via

SEM micrographs. Diamond 3.2 software has been used for the crystal structure of the synthesized sample.

2.6 Conduction Mechanisms

In the present thesis, two conduction mechanism has been used to understand the current-voltage (*I-V*) hysteresis behaviors.

2.6.1 Space Charge Limited Current (SCLC)

SCLC is the bulk of the limited conduction mechanism and shows how the conduction current (I) behavior is changing with increasing electric field.

At a lower voltage, the current density (*J*) is proportional to the electric field ($J = ne\mu E$), which shows the Ohmic current. When the applied voltage is increased, charges accumulate in the region between the electrodes and the electric field as the accumulated charge affects the conduction current. This mechanism is usually indicated the SCLC and is given by [137].

$$J = 9\varepsilon \mu V^2/8d^3$$

where V is the applied voltage, d is the thickness of the materials, ε is the static dielectric constant, n is the concentration of the free charge carriers in thermal equilibrium, and μ is the mobility. For space-charge-limited current, *J-V* characteristic plotted in a log-log curve is shown in Fig. 2.16. Ohm's law ($J_{Ohm} \propto V$), Child's law ($J_{Child} \propto V^2$), and traps-filled limit (TFL) current ($J_{TFL} \propto V^2$) are the three curves of the *J-V* characteristic in a log (*J*)-log(*V*). The transition voltage is V_{tr} and V_{TFL} at the departure from ohm's law and TFL curve, respectively:

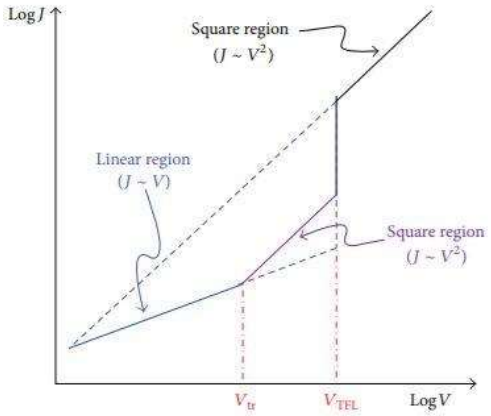

Figure 2.16: J-*V* characteristic of SCLC [138].

2.6.2 Poole-Frenkel

Poole-Frenkel is used to understand the trapping and de-trapping process of the synthesized sample. This mechanism is very similar to that of Schottky emission. Therefore, Poole–Frenkel is called internal Schottky emission because thermal excitation of electrons can be emitted from the trap into the conduction of the dielectric [139]. In this thesis work, the Poole-Frenkel has been used to calculate the trapped energy. Poole-Frenkel relation is given by [140].

$$\sigma_E = k_2\, e^{-\beta \varepsilon_{trap}}$$

$$k_2 = q\mu N_c\, e^{\left(\frac{\beta \Delta E_{cB,vB}}{2}\right)}$$

$$\varepsilon_{trap} = q(\phi_B - \sqrt{(qk_e/\varepsilon_r)E}$$

The variation of the relative dielectric constant was obtained from the slope ($E^{1/2}$ *vs ln* σ) of F-P fitting in forward and reverse scanning using current-voltage data.